Vacuum 129 (2016) 45–48

Contents lists available at ScienceDirect

Vacuum

journal homepage: www.elsevier.com/locate/vacuum

Nanoscale interwoven structure of B2 and R-phase in Ni–Ti alloy film

Chunwang Zhao [a, b, *], Shilei Zhao [b], Yongjun Jin [b], Xiaokai Meng [b]

[a] College of Arts and Sciences, Shanghai Maritime University, Shanghai, 201306, China
[b] College of Science, Inner Mongolia University of Technology, Hohhot, 010051, China

ARTICLE INFO

Article history:
Received 1 February 2016
Received in revised form
13 April 2016
Accepted 13 April 2016
Available online 14 April 2016

Keywords:
Ni-Ti
R-phase
Sputtering
Thin film
Transmission electron microscopy

ABSTRACT

Ti–50.3Ni (at%) alloy film was prepared by vacuum magnetron sputtering, followed by heat treatment at 460 °C for 40 min. The microstructure of the Ni–Ti alloy film was studied using transmission electron microscopy. A nanoscale interwoven structure of B2 and R-phase was observed. The lattice correspondences between B2 and R-phase were analyzed using an electron diffraction pattern. The R-phase can nucleate in the precipitate-free area of the Ni–Ti alloy film at a rapid cooling condition. The full-field strain of B2 and R-phase was mapped through geometric phase analysis technique. The measured strains are consistent with the eigenstrains of the R-phase.

Shape memory alloy (SMA) with shape memory effect and superelasticity, which is used for engineering applications, has gained considerable research attention in recent decades [1]. Ni–Ti alloy is the most popular SMA. The high-temperature austenitic parent phase of Ni–Ti alloy exhibits a B2 cubic structure, whereas the low-temperature martensite phase displays a B19′ monoclinic structure [2]. The martensite transformation from a high-temperature phase to a low-temperature phase can undergo two paths. One is 1-stage B2 ↔ B19′ transformation, and the other is 2-stage B2 ↔ R ↔ B19′ transformation. The intermediate R refers to the so-called R-phase. The occurrence of 1-stage transformation or 2-stage transformation depends on the composition and heat treatment history of Ni–Ti alloy [3]. Fukuda et al. proposed that R-phase nucleations occur at certain stress-concentrated sites, such as matrix–precipitate interfaces and dislocation. A self-accommodation mechanism of R-phase in Ti–48.2Ni–1.5Fe (at%) and Ti–48Ni–2Al was presented through in-situ transmission electron microscopy (TEM) observation [4]. Tan et al. [5] studied the phase transformation of Ti-50.7Ni alloy through in-situ TEM and found that the Ni–Ti alloy appeared in two-stage phase transformation after aging treatment at 550 °C for 20 min. Microstructural analysis showed that $Ti_{11}Ni_{14}$ precipitates appeared during aging treatment, which resulted in R-phase transformation at the boundaries between the precipitates and the matrix. Moreover, Tan et al. found a new morphology of interwoven austenite/martensitic structure at a rapid cooling condition [5]. Tirry et al. proposed that the strain field surrounding the precipitates, which is caused by the matrix–precipitate lattice mismatch, is a possible reason for R-phase nucleation. The strain field of the phase boundary between Ni_4Ti_3 precipitates and B2 matrix was determined and compared with the eigenstrain of R-phase, and a consistent conclusion was obtained [6].

Therefore, R-phase nucleation is believed to always originate from stress/strain-concentrated sites, such as matrix–precipitate interface or dislocation, and then R-phase grows gradually from the stress/strain-concentrated sites to the parent phase [3,4]. In the present study, a nanoscale interwoven structure of B2 and R-phase in Ni–Ti alloy film was observed, and the nucleation mechanism of R-phase was analyzed.

The Ni–Ti alloy film was prepared by vacuum magnetron sputtering with two targets of Ti and Ti–50Ni. The substrate was a silicon wafer coated with 100 nm-thick silicon nitride film. The base vacuum was 4.0×10^{-5} Pa. The film thickness was measured to be approximately 1.5 μm by scanning electron microscopy (SEM). The film composition was determined to be Ti–50.3Ni by energy-dispersive spectrometry equipped in SEM. The film was subjected to heat treatment at 460 °C for 40 min in a vacuum tube furnace,

* Corresponding author. College of Arts and Sciences, Shanghai Maritime University, Shanghai, 201306, China.
E-mail address: cwzhao@shmtu.edu.cn (C. Zhao).

http://dx.doi.org/10.1016/j.vacuum.2016.04.015
0042-207X/

followed by rapid cooling with an air fan. After heat treatment, the Ni–Ti alloy film was peeled off the substrate and glued at a TEM copper ring. Ar^+ milling was applied to the film at low bombardment energy and a small angle until perforation. The microstructure was then studied with a JEM-2010 TEM at 200 kV. TEM images were recorded with a Gatan 1k × 1k CCD and processed using the DigitalMicrograph software. The strain field was mapped using GPA Phase software, which is a plugin of the DigitalMicrograph software. The simulated electron diffraction image was calculated using JEMS software. An X-ray diffraction (XRD) experiment was performed using a D8 Advanced diffractometer.

Fig. 1 depicts the XRD pattern of the annealed sample. The diffraction peaks were identified carefully and the corresponding crystal plane indexes were marked on the XRD peaks. It can be seen that there are only NiTi B2 and R-phase without other phases like Ti_3Ni_4. Fig. 2a depicts the TEM bright field image of the grains in the Ni–Ti alloy film. As shown in the figure, the Ni–Ti alloy film is in polycrystalline state with an average grain size of 2.2 μm. The contrast of the grains is not homogeneous, and some strip-shaped areas in the interior of the grains exist. To analyze the microstructure and the phases of the grains in detail, a white boxed area in Fig. 2a was further observed in a higher magnification, and its TEM image is shown in Fig. 2b. A nanoscale interwoven structure consisting of strip-shaped areas is clearly shown. The strip-shaped areas can be identified to be two morphologies, which are wide strip areas with an average width of 32 nm and narrow strip areas with an average width of 12 nm.

To determine the phases of the interwoven structure, the electron diffraction pattern of the observed area was obtained (Fig. 2c). After measuring the relative position of these diffraction spots, we determined that three sets of diffraction spots coexist in Fig. 2c. The large bright diffraction spots mainly come from B2 (its reduced quadrangle is marked by white lines) at [113] zone axis. The indexes of the diffraction spots of B2 are illustrated in the corresponding simulated electron diffraction pattern in Fig. 2d. The medium-sized diffraction spots come from R-phase (its reduced quadrangle is marked by yellow lines in the web version) at $[\bar{1}15]$ zone axis. The indexes of the diffraction spots of R-phase are illustrated in the corresponding simulated electron diffraction pattern in Fig. 2e. The orientation relations between B2 and R-phase can be decided by the position of the diffraction spots: $\bar{1}10_{B2}//\bar{3}2\bar{1}_R, 2\bar{1}1_{B2}//\bar{3}30_R, 1\bar{2}1_{B2}//0\bar{5}1_R$. The small diffraction spots (marked by the red arrow in the web version) also come from the R-phase but at [015] zone axis. The indexes of the diffraction spots are illustrated in the corresponding simulated electron diffraction pattern in Fig. 2f. The orientation relations between B2 and R-phase can be decided by the position of the diffraction spots: $\bar{1}10_{B2}//300_R$.

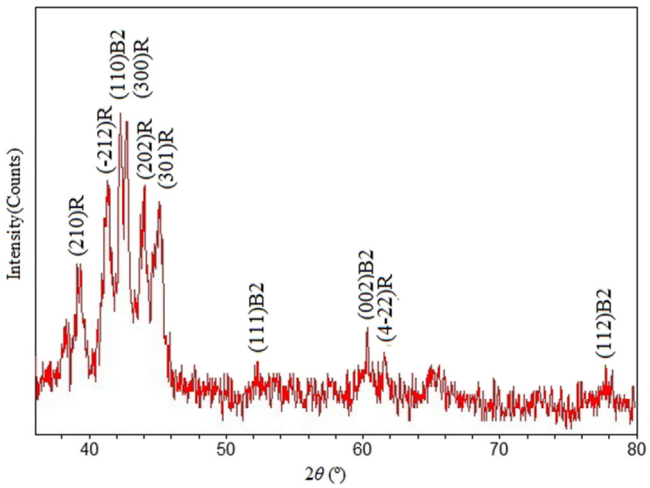

Fig. 1. XRD pattern of the Ni–Ti alloy film.

Fig. 3a depicts the high-resolution transmission electron microscopy (HRTEM) image of the white boxed area in Fig. 2b. Fig. 3b is the corresponding fast Fourier transformation (FFT) image of the HRTEM image in Fig. 3a, which is similar to the electron diffraction pattern in Fig. 2c, but it does not show small diffraction spots. According to the measurement for the interplanar spacing and the included angle of the crystal planes, the observed area in Fig. 3a comprises two phases: one is B2, which is located at the upper left side and lower right side of the HRTEM image (marked by letter B2), whereas the other strip area from the lower left to the upper right is R-phase (marked by letter R). Therefore, according to the electron diffraction pattern and the HRTEM image, the wide strip areas in Fig. 2b refer to B2, and the narrow strip areas refer to R-phase. By selecting the $\bar{1}10_{B2}/\bar{3}2\bar{1}_R$ and $2\bar{1}1_{B2}/\bar{3}30_R$ diffraction spots in Fig. 3b and conducting a filtering and inverse FFT processing, the crystal planes of $\bar{1}10_{B2}/\bar{3}2\bar{1}_R$ and $2\bar{1}1_{B2}/\bar{3}30_R$ can be extracted, as shown in Fig. 3c and d. The paralleled relation between B2 and R-phase can also be observed directly.

Subsequently, the strains perpendicular to $\bar{1}10_{B2}/\bar{3}2\bar{1}_R$ and $2\bar{1}1_{B2}/\bar{3}30_R$ were mapped using the geometric phase analysis (GPA) technique [7] from the HRTEM image (Fig. 3a) and are shown in Fig. 3e and f, respectively. When using GPA to calculate a strain field, a reference area, which is supposed to be strain-free, must be selected. Briefly, the full-field strains are actually relative strains. In this work, a rectangular reference area was selected in the lower right B2 area, as shown in Fig. 3e. The different colors in the strain field maps represent the different strain values, which can be identified with the color scale. Moreover, the color scale indicates strain changes from −15% to +15%. Many 8-shaped areas (marked with white arrows) exist in Fig. 3e and 3f, which are very similar with the strain field of dislocations [8]. In current case, however, we think that the 8-shaped areas cannot provide valid information because the lattice fringes of the corresponding areas in the original HRTEM image (Fig. 3a) are not clear enough. As shown in Fig. 3c, lattice fringes of $\bar{3}2\bar{1}_R$ are not clear enough because the zone axis of the R-phase was not strictly parallel to the electron beam of the TEM. Therefore, we failed to obtain an informative strain field in the R-phase area. However, the partial boundaries between the R-phase and B2 are clear enough, and a strain of 2.4% can be obtained, as marked in Fig. 3e. Meanwhile, the lattice fringes of $\bar{3}30_R$ are clear enough, as shown in Fig. 3d. Thus, a relatively ideal strain field of the R-phase area has been obtained, and the average strain is measured to be −0.57%, as marked in Fig. 3f. The lattice constant of bulk NiTi B2 is $a_{B2} = 0.3014$ nm, whereas the lattice constants of bulk NiTi R-phase are $a_R = 0.7339$ nm and $c_R = 0.5284$ nm [9]. Thus, the eigen interplanar spacings of B2 can be calculated as follows: $d_{\bar{1}10_{B2}} = 0.2131$ nm, and $d_{2\bar{1}1_{B2}} = 0.1230$ nm. The eigen interplanar spacings of the R-phase can be calculated as $d_{\bar{3}2\bar{1}_R} = 0.2187$ nm and $d_{\bar{3}30_R} = 0.1223$ nm. These data indicate that the eigen interplanar spacings of B2 and R-phase are not identical. Hence, the small differences between these crystal planes are the eigenstrains. The relative strains of the R-phase perpendicular to each crystal planes can be calculated as follows:

$$\varepsilon_{\bar{3}2\bar{1}_R} = \frac{d_{\bar{3}2\bar{1}_R} - d_{\bar{1}10_{B2}}}{d_{\bar{1}10_{B2}}} = \frac{0.2187 - 0.2131}{0.2131} \times 100\% = 2.6\%$$

and